RSC Advances

PAPER

View Article Online
View Journal | View Issue

Cite this: *RSC Adv.*, 2017, **7**, 9009

The novel and facile preparation of multilayer MoS_2 crystals by a chelation-assisted sol–gel method and their electrochemical performance

Xingzhong Guo,* Zichen Wang, Wenjun Zhu and Hui Yang*

Received 20th October 2016
Accepted 23rd January 2017

DOI: 10.1039/c6ra25558b

rsc.li/rsc-advances

Multilayer molybdenum disulfide (MoS_2) was facilely prepared by a chelation-assisted sol–gel method with ammonium molybdate tetrahydrate ($(NH_4)_6Mo_7O_{24}\cdot 4H_2O$) as the molybdenum source, thioacetamide (CH_3CSNH_2) as the sulfur source and diethylenetriamine pentaacetic acid (Dtpa) as the chelating agent, subsequently followed by high-temperature calcination. The chelating agent Dtpa ingeniously mediated the chelation reaction of the system and promoted the formation of a monolithic gel. The hexagonal MoS_2 crystal (2H-MoS_2) with good crystallinity precipitated after calcination at 1000 °C with the Mo and S mass ratio of 1 : 3. The adjustable MoS_2 layers stacked together to form MoS_2 flakes, and these flakes aggregated to construct crystalline MoS_2 particles. The electrochemical tests showed the possibility of as-prepared MoS_2 crystals applied as a negative electrode for lithium ion batteries.

1. Introduction

Molybdenum disulfide (MoS_2) is a type of layered compound with a graphene-like structure, and has been widely applied in electrochemical, optical and mechanical fields due to its special structure and excellent properties.[1,2] Structurally, MoS_2 crystals are stacked by S atom layers and Mo atom layers arranged alternately where every Mo atom connects six S atoms with covalent bonds, and the adjacent layers interact by van der Waals force.[3,4]

Up to now, a series of MoS_2 with different nanostructures such as nanosheets, nanoflowers, microspheres and monolayered MoS_2 sheets have been used in lithium ion battery storage due to the high reversible capacity (up to 1290 mA h g^{-1}). Ding *et al.* successfully prepared MoS_2 microspheres with good initial discharge and charge capacities (1160 and 791 mA h g^{-1}) and a capacity of 672 mA h g^{-1} after 50 cycles.[5] Lin *et al.* produced sulfur-depleted monolayered MoS_2 nanocrystals by exfoliating and disintegrating the bulk MoS_2 and the products showed excellent catalytic performance on HER.[6] Chhowalla *et al.* demonstrated that metallic 1T phase MoS_2 nanosheets prepared by chemical exfoliation can intercalate ions such as H^+, Li^+ and Na^+ efficiently and reach capacitance values from 400 to ~700 F cm^{-3}.[7] Hu *et al.* synthesized MoS_2 nanoflowers with expanded interlayers and used the products as Na-ion battery anode with high discharge capacities and good rate capability.[8] Wang *et al.* prepared single-layer MoS_2/graphene composites as the anode electrode of lithium ion battery with better cycle performance and rate capability than pure MoS_2 electrode due to the good electron conductivity of graphene and the synergy effect between MoS_2 and graphene.[38]

There have been various synthetic methods to prepare MoS_2 and its composites, including hydrothermal synthesis, solid-state process, chemical vapor deposition (CVD), *etc.*[9–11] Wherein, hydrothermal synthesis is a common method for the preparation of well-crystallized MoS_2 with various morphologies due to high temperature and pressure conditions.[12,13] However those preparation methods almost are expensive, complicated and low productive. Sol–gel method is a new synthetic route for advanced materials based on low-temperature, high production, moderate reacting conditions and molecular-level mixture.[14] So sol–gel method could be a cheap and simple way to prepare MoS_2 crystal. At present, only Li *et al.* reported the preparation of porous MoS_2 *via* a sol–gel route using $(NH_4)_2Mo_3S_{13}$ as precursor.[15] However, the dissolving reaction of the precursor $(NH_4)_2Mo_3S_{13}$ to prepare "Mo_3S_{12}" gel is not supposed to be real sol–gel process. In addition, the precursor $(NH_4)_2Mo_3S_{13}$ is quite rare and very hard to synthesize. Therefore, it is essential to develop an effective and low-cost sol–gel approach to prepare MoS_2 materials.

In the present work we demonstrate a novel and facile chelation-assisted sol–gel method to prepare multilayer MoS_2. The common and inexpensive ammonium molybdate tetrahydrate ($(NH_4)_6Mo_7O_{24}\cdot 4H_2O$), thioacetamide ($CH_3CSNH_2$) and diethylenetriamine pentaacetic acid (Dtpa) were employed as molybdenum source, sulfur source and chelating agent, respectively. The mass ratio of Mo and S has an important role on the formation of multilayer MoS_2 crystalline phase. The synthesis mechanism, surface morphology, crystal structure and electrochemical performances of the as-prepared MoS_2 were also studied.

School of Materials Science and Engineering, Zhejiang University, Xihu District, Hangzhou, 310027, China. E-mail: msewj01@zju.edu.cn; yanghui@zju.edu.cn; Fax: +86-571-8795-3054; Tel: +86-571-87953313; +86-571-8795-1408

2. Experimental

2.1. Preparation of MoS_2

All reagents are purchased from Aladdin Industrial Corporation and are AR (analytically pure) level. Three typical experiments were carried out and the corresponding samples were named as MoS_2-1, MoS_2-2 and MoS_2-3, which are different in the amount of S source. For the preparation of MoS_2-1, 0.2 g (0.16 mmol) ammonium molybdate tetrahydrate ($(NH_4)_6Mo_7O_{24}\cdot 4H_2O$) was firstly dissolved in 8 mL deionized water, and then 0.4 g (5.32 mmol) thioacetamide (CH_3CSNH_2) was added into the solution under continuous stirring. 0.05 g diethylenetriamine pentaacetic acid (Dtpa) was added into the solution to obtain the brown sol under stirring for 1 h. The sol was transferred into 60 °C oven for 12 h to gelate into bronze gel and kept drying at 60 °C for two days. After drying, some of the xerogel was calcinated in the tube furnace at 1000 °C for 4 h in a stream of argon flowing at 180 sccm to form 2H-MoS_2 phase. MoS_2-2 and MoS_2-3 were synthesized in the same process with the amounts of CH_3CSNH_2 of 0.6 and 0.8 g respectively.

2.2. Characterization

The X-ray diffraction (XRD) patterns of the samples were carried out on an X'Pert Pro diffractometer with a Cu Kα radiation (λ = 0.15418 nm). The step size is 0.02626°, the time per step is 25.5 s, and the total scan time is 4 min 42 s without any mask or filters. Raman spectra were performed on the Renishaw InVia Raman microscope under the excitation length of 532 nm. The morphologies and microstructures of the samples were observed by Hitachi S-4800 scanning electron microscopy (SEM) operating at 3.0 kV and JEOL 2100F transmission electron microscopy (TEM) at an acceleration voltage of 200 kV. Electrochemical measurements were performed using CR 2025 coin cells. The preparation process of SEM samples are as follows. At first, samples were dispersed homogeneously in ethyl alcohol with ultrasonic processing. Then the suspension liquid were dropped onto the aluminum foil. After the ethyl alcohol volatilized, the samples were left on the aluminum foil. The preparation process of TEM samples was the same as the SEM one except the objective table was copper grid. The working electrode was prepared by coating the slurry (80 wt% of active materials, 10 wt% of carbon black, and 10 wt% of polyvinylidene fluoride binder in *N*-methyl-2-pyrrolidinone) onto a Cu foil and dried in a vacuum oven at 120 °C for 12 h. A lithium foil was used as the counter electrode, a mixture of 1 M $LiPF_6$ in ethylene carbonate (EC)–dimethyl carbonate (DMC) (1 : 1 by volume) was employed as the electrolyte and a polypropylene microporous film was applied as the separator. Cell assembly was conducted in an argon-filled glovebox with oxygen and water concentration below 1 ppm. The galvanostatic charge/discharge measurements were carried out in a Land battery testing system in the voltage range of 0.001–3 V (*vs.* Li^+/Li). The cyclic voltammetry (CV) tests were performed between 0.05 V and 3.0 V at a scan rate of 0.2 mV s^{-1} on a CHI660C electrochemical workstation (Shanghai Chenhua, China). The electrochemical impedance spectroscopy (EIS) measurements were tested on the same workstation with the frequency ranging from 0.01 Hz to 100 kHz.

3. Results and discussion

Fig. 1 shows the synthesis mechanism of multilayer MoS_2 by chelation-assisted sol–gel method with diethylenetriamine pentaacetic acid (Dtpa) as chelating agent. Firstly, amounts of $[Mo_7O_{24}]^{6-}$ ionic groups existed in the neutral solution. $[Mo_7O_{24}]^{6-}$ is composed of seven octahedral $[MoO_6]$ ionic groups where three different bond lengths exist between Mo and O atoms.[39,40] Then the S^{2-} ions provided by CH_3CSNH_2 substituted for the terminal O atoms combined by Mo–O ionic bond because the bond energy of Mo–S is higher than that of terminal Mo–O. After adding Dtpa into the solution, the chelating agent attacked some new S atoms, broke the Mo–S bonds, and chelated with Mo atoms which lacked electrons to form stable electron structure. In the process, some of the S source were lost in the form of H_2S. Every Dtpa molecule connected three Mo atoms of different $Mo_7O_{24}^{6-}$ ionic groups to form a complicated network structure, which promoted the formation of gel. The wet gel gradually formed at 60 °C in 12 h. Then it transformed into xerogel in two days when the water was totally evaporated and the shrinkage happened in the range between 40% and 60% of the original size. The crystallization of the complex gel was conducted by calcinations at 1000 °C, and the multilayer MoS_2 can be facilely obtained.

The XRD patterns of as-prepared samples show the precipitates are hexagonal 2H-MoS_2 (JCPDS 37-1492) with different crystallinity (Fig. 2). It is obvious that the MoS_2-2 sample displays the sharpest diffraction peaks, indicating the highest crystallinity. It reveals that complete MoS_2 crystal tends to be formed when the mass ratio of Mo source and S source is 1 : 3. The diffraction peak of MoS_2-2 sample at $2\theta = 14.2°$ indicates the MoS_2 layers stack orderly along (002) direction with a *d*-spacing of 0.62 nm. The (100) reflection at $2\theta = 33.5°$ and (110) reflection at $2\theta = 59.1°$ can be found in MoS_2-3 sample but no clear (002) reflection. It is supposed that some complicated polysulfide molybdenum were synthesized owing to redundant

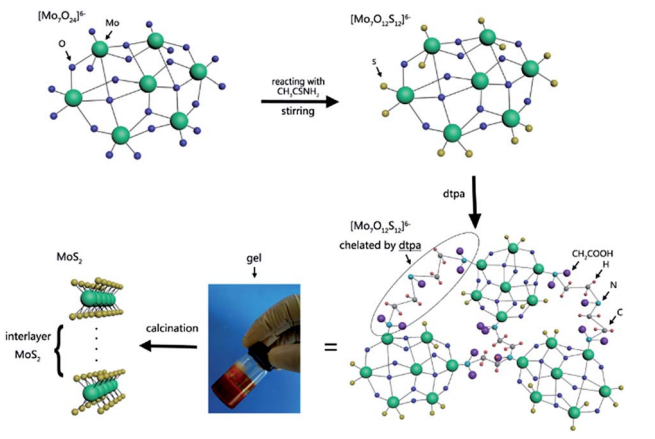

Fig. 1 Preparation process of MoS_2 by sol–gel method assisted by Dtpa.

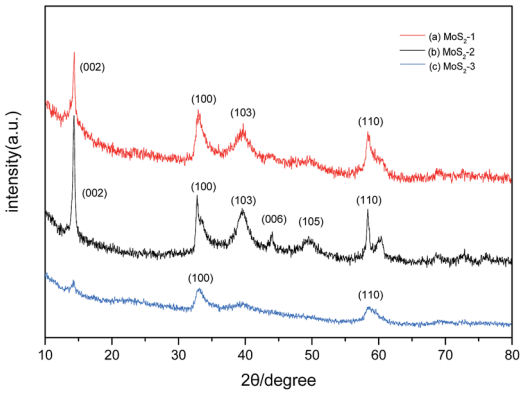

Fig. 2 XRD patterns of as-prepared samples.

S source in MoS_2-3 sample and few MoS_2 layers are stacked in the c direction.[16] According to the Scherrer formula, $D = K\lambda/B\cos\theta$, $K = 0.89$, $\lambda = 0.154056$ nm, $\theta = 14.2°$, $B = 0.507$ for MoS_2-2 and $B = 0.591$ for MoS_2-1. The average dimension of MoS_2 in z-axis is roughly estimated at about 15 nm in MoS_2-2 sample corresponding to 25 MoS_2 layers, which was facilitated by high-temperature calcination. For MoS_2-1 sample, the MoS_2 grain dimension in z-axis is about 13 nm, corresponding to 21 MoS_2 layers approximately. It shows that the mass ratio of Mo and S plays a role on the formation of multilayer MoS_2 to some extent.

The three samples were further investigated to analyze the inner structure by Raman spectroscopy (Fig. 3). It has been proved that E^1_{2g} and A_{1g} peaks of monolayer MoS_2 appear at 384.3 and 403 cm^{-1}, respectively.[17] With the increase of layer numbers, the in-plane E^1_{2g} vibration weakens and the out-of-plane A_{1g} vibration strengthens. When the layer number is over 6, the E^1_{2g} and A_{1g} peaks are observed at 382 and 408 cm^{-1} stably.[18,19] It is seen that the MoS_2-2 sample exhibits a strong out-of-plane vibration at 408 cm^{-1} and a relatively weaker in-plane vibration at 382 cm^{-1}. However, the signal of this Raman spectroscopy is a little weak and red shifts are found in MoS_2-1 and MoS_2-3 samples. It is supposed that amorphous substances and defects in the resultant sample disorder the uniform MoS_2 molecule vibrations, thus causing these phenomena. Due to the selection rules for scattering geometry and limited rejection of the Raleigh scattered radiation, the other two vibration modes E_{1g} and E^2_{2g} could not be detected.[20] It proves that the mass ratio of Mo and S also impacts the inner structure of as-prepared MoS_2.

The microstructures and morphologies of as-prepared MoS_2-2 sample were observed by SEM and TEM (Fig. 4). It is seen that the MoS_2 precipitates exist in the form of particles with the size of <2 μm and some agglomeration (Fig. 4a). Fig. 4b depicts irregular MoS_2 flakes aggregate together to form larger particles. As shown in Fig. 4c, the MoS_2 nanosheets stack together to form a large flake with different inside thickness. It is clearly observed from Fig. 4d that a nanosheet has some parallel MoS_2 crystal fringes with an interlayer distance of 0.62 nm, corresponding to interplanar spacing of 2H-MoS_2 (002) plane based on XRD results. The high magnification HR-TEM image of the thin MoS_2 layers (Fig. 4e) confirms that the as-prepared MoS_2 is typically hexagonal MoS_2. The interlayer distance of (100) plane and (110) plane are 0.27 and 0.16 nm, respectively. The selected area electron diffraction (SAED) (Fig. 4f) shows a clear monocrystalline MoS_2 diffraction pattern with six inner diffraction spots indicating (100) plane and the outer diffraction spots indicating (110) plane. There is no (002) plane diffraction spots because the electrons incident direction is [001]. Based on above analysis, during the formation of MoS_2 particles, large amounts of monocrystalline MoS_2 layers in different orientations stacked to form nanosheets, the multilayer nanosheets

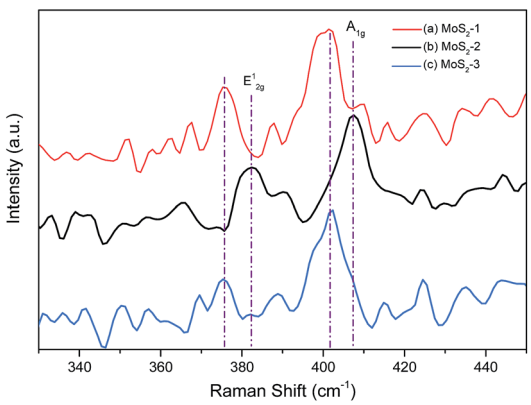

Fig. 3 Raman spectroscopy of as-prepared samples.

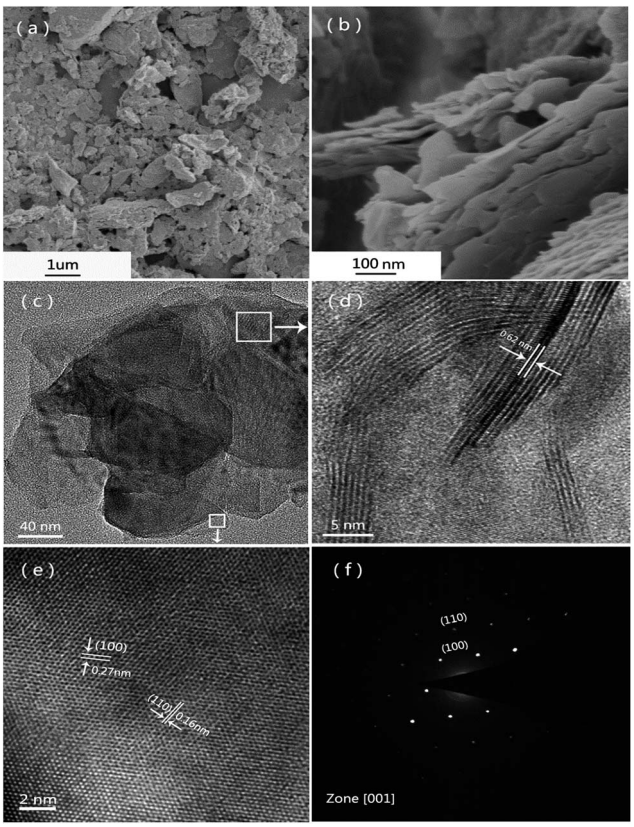

Fig. 4 SEM and TEM photos of as-prepared sample MoS_2-2.

arranged to form MoS_2 flakes, and then the flakes aggregated to construct crystalline MoS_2 particles.

We used the sample MoS_2-2 as the negative electrode of lithium ion battery because of its superior structure and composition. Fig. 5 depicts the cyclic voltammetry (CV) profile of as-prepared sample MoS_2-2. Cyclic voltammetry is a normal method to research the redox reactions of the electrodes. From Fig. 5, two obvious reduction peaks at 0.6 V and 0.4 V are shown in the first cycle. The peak at 0.6 V implies intercalation of lithium ions into MoS_2 layers with MoS_2 structure transformation from 2H (trigonal prismatic coordination) to the 1T (octahedral coordination).[21–23] The other peak at 0.4 V can be attributed to the conversion reaction process of Li_xMoS_2 into Mo and Li_2S. In the anodic sweep, the peak in 2.25 V is attributed to the delithiation of Li_2S with the reaction process of $Li_2S - 2e \rightarrow 2Li^+ + S$.[7,24,25] In the second and third cathodic sweep, three reduction peaks are found at 1.7 V, 1.0 V, and 0.2 V, respectively, which could be due to the following reactions: $2Li^+ + S + 2e \rightarrow Li_2S$, $MoS_2 + xLi^+ + xe \rightarrow Li_xMoS_2$, and $Li_xMoS_2 + (4 - x)Li^+ + (4 - x)e \rightarrow Mo + 2Li_2S$.[26,27]

Fig. 6 shows the first three charge–discharge profiles of the sample MoS_2-2 electrodes with a cutoff voltage of 0.005–3 V at a current density of 100 mA g^{-1}, which are nearly accord with the CV measurements described above. In the first discharge process, there are two obvious voltage plateaus at 0.5 V and 1.0 V, which indicates the formation of Li_xMoS_2 and the following conversion reaction of Li_xMoS_2 into Mo and Li_2S.[1,17,28] The slope region below 0.5 V could be attributed to the formation of a solid-electrolyte interphase (SEI) layer.[29,30] In the second and third discharge process, three vague potential plateaus could be found at 1.7 V, 1.0 V and 0.25 V, which are in qualitative agreement with the CV results. In the charge process, the MoS_2-2 electrode shows a distinct potential plateaus at 2.25 V, which could be due to the reduction of sulfur to polysulfide.[24,31,32] Fig. 6 also shows that the MoS_2-2 electrode delivers an initial discharge capacity of 1149 mA h g^{-1} and a reversible charge capacity of 1038 mA h g^{-1}, with a high coulombic efficiency of 90.3%.

Fig. 7a depicts the cycling behavior and rate capability of the sample MoS_2-2 at a constant current density of 100 mA g^{-1}. Although the first charge and discharge capacities are higher

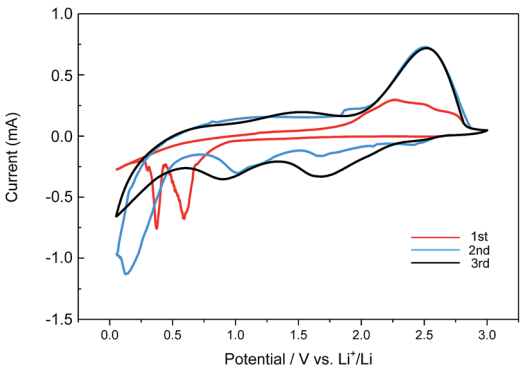

Fig. 5 The first three cyclic voltammograms of as-prepared sample MoS_2-2.

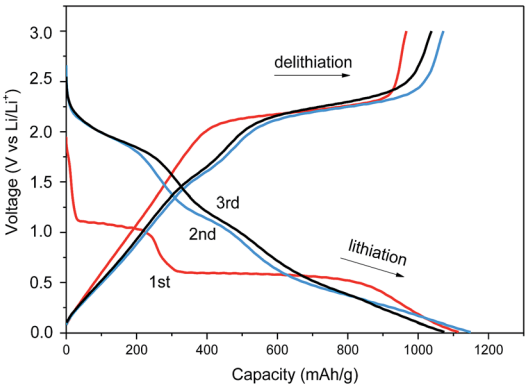

Fig. 6 Galvanostatic charge and discharge curves of as-prepared sample MoS_2-2 at a current density of 100 mA g^{-1}.

than 900 mA h g^{-1}, the cycling stability of the MoS_2-2 electrode is poor with a discharge capacity decrease from 947 to 353 mA h g^{-1} after 40 cycles. Fig. 7b shows the rate cycling behavior of the sample MoS_2-2 electrode. At the current densities of 1.0 A g^{-1}, the capacity rapidly declines below 300 mA h g^{-1}, which cannot compete with the MoS_2/graphene composite electrode with good rate performance. Surprisingly, the sample MoS_2-2 electrode has a high coulombic efficiency of nearly 100%.

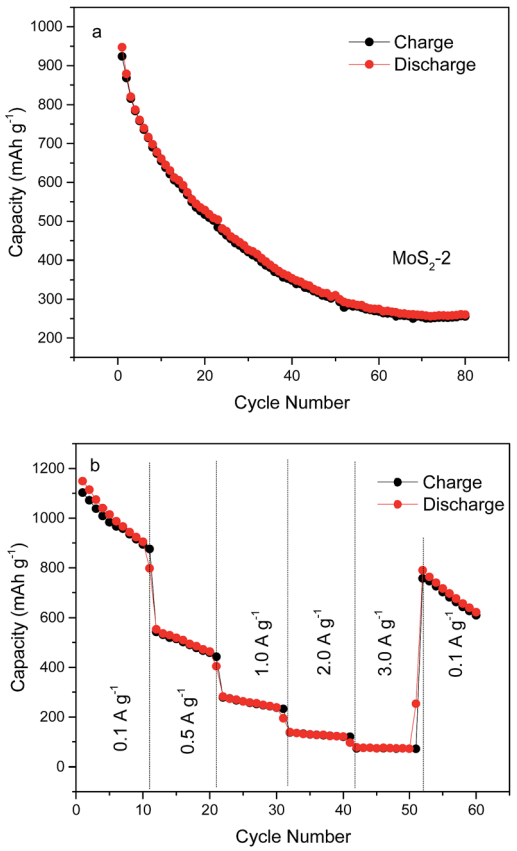

Fig. 7 (a) Cycle performance of as-prepared sample MoS_2-2 electrode at a current density of 0.1 A g^{-1}, and (b) their rate capabilities at different current densities.

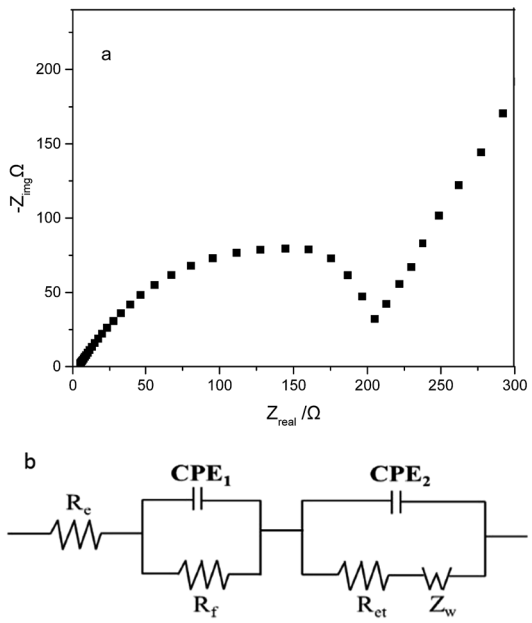

Fig. 8 (a) Nyquist plots of as-prepared sample MoS_2-2 electrode in the frequency range from 200 kHz to 0.01 Hz; and (b) an equivalent circuit model of the electrode, CPE is the constant phase element, $Z_{CPE} = \{Q(jw)^n\}^{-1}$, $0 < n < 1$.

Electrochemical impedance spectra (EIS) can be applied to better understand the electrochemical performance of MoS_2 electrode. Fig. 8a depicts the Nyquist plots of MoS_2-2 electrode after 40th cycle, and Fig. 8b is the equivalent circuit model for the impedance response. The semicircle in high-frequency region is due to the resistance R_f and CPE_1 of the solid electrolyte interphase (SEI) film.[33,34] The medium-frequency semicircle corresponds to the charge-transfer resistance R_{ct} and CPE_2 of the electrode/electrolyte interface.[35,36] The inclined line is assigned to the lithium-diffusion within the electrode material.[37] According to EIS equivalent circuit in Fig. 8b, R_f and R_{ct} of MoS_2-2 electrode are 14.84 and 121.9 Ω, respectively.

4. Conclusions

In summary, the multilayer MoS_2 crystal was synthesized by a chelation-assisted sol–gel method followed by calcination. Diethylenetriamine pentaacetic acid (Dtpa) as chelation agent was introduced to react with Mo and S sources to form Mo–S chelated gel. The mass ratio of Mo and S affected the formation of multilayer MoS_2 as well as the inner structure of MoS_2, and the best crystalline MoS_2 particles are obtained with the Mo and S mass ratio of 1 : 3. The resultant crystalline MoS_2 particles were constructed by irregular MoS_2 flakes arranged together, while these flakes were formed by adjustable MoS_2 layers stacked together. The electrochemical tests showed the possibility of as-prepared MoS_2 applied as negative electrode for lithium ion batteries. In order to improve the electrochemical performance, we need to continually explore a sol–gel process to prepare MoS_2/graphene composite with the aid of synergy effect between MoS_2 and graphene and the superior electron conductivity of graphene.

Acknowledgements

This work is supported by the National Natural Science Foundation of China (51372225) and High Science & Technique Brainstorm Project of Zhejiang Province of China (No. 2017C01002).

References

1 Z. Wang, T. Chen, W. Chen, K. Chang, L. Ma, G. Huang, D. Chen and J. Y. Lee, *J. Mater. Chem. A*, 2013, **1**, 2202.
2 M. A. Worsley, S. J. Shin, M. D. Merrill, J. Lenhardt, A. J. Nelson, L. Y. Woo, A. E. Gash, T. F. Baumann and C. A. Orme, *ACS Nano*, 2015, **9**, 4698.
3 A. K. Geim and I. V. Grigorieva, *Nature*, 2013, **499**, 419.
4 Q. H. Wang, K. Kalantar-Zadeh, A. Kis, J. N. Coleman and M. S. Strano, *Nat. Nanotechnol.*, 2012, **7**, 699.
5 S. J. Ding, D. Y. Zhang, J. S. Chen and X. W. Lou, *Nanoscale*, 2012, **4**, 95.
6 L. Lin, N. Miao, Y. Wen, S. Zhang, P. Ghosez, Z. Sun and D. A. Allwood, *ACS Nano*, 2016, **10**, 8929.
7 M. Acerce, D. Voiry and M. Chhowalla, *Nat. Nanotechnol.*, 2015, **10**, 313.
8 Z. Hu, L. Wang, K. Zhang, J. Wang, F. Cheng, Z. Tao and J. Chen, *Angew. Chem.*, 2014, **53**, 12794.
9 J. Brivio, D. T. Alexander and A. Kis, *Nano Lett.*, 2011, **11**, 5148.
10 X. L. Li and Y. D. Li, *Chemistry*, 2003, **9**, 2726.
11 L. Ma, W.-X. Chen, Z.-D. Xu, J.-B. Xia and X. Li, *Nanotechnology*, 2006, **17**, 571.
12 H. Lin, X. Chen, H. Li, M. Yang and Y. Qi, *Mater. Lett.*, 2010, **64**, 1748.
13 W.-J. Li, E.-W. Shi, J.-M. Ko, Z.-z. Chen, H. Ogino and T. Fukuda, *J. Cryst. Growth*, 2003, **250**, 418.
14 X. Guo, Q. Zhang, X. Ding, Q. Shen, C. Wu, L. Zhang and H. Yang, *J. Sol-Gel Sci. Technol.*, 2016, **79**, 328.
15 N. Li, Y. Chai, B. Dong, B. Liu, H. Guo and C. Liu, *Mater. Lett.*, 2012, **88**, 112.
16 X. Y. Zhao, C. W. Hu and M. H. Cao, *Chem.–Asian J.*, 2013, **8**, 2701.
17 L. Ma, X. Zhou, L. Xu, X. Xu, L. Zhang and W. Chen, *Electrochim. Acta*, 2015, **167**, 39.
18 C. Lee, H. Yan, L. E. Brus, T. F. Heinz, J. Hone and S. Ryu, *ACS Nano*, 2010, **4**, 2695.
19 G. L. Frey, R. Tenne, M. J. Matthews, M. S. Dresselhaus and G. Dresselhaus, *Phys. Rev. B: Condens. Matter Mater. Phys.*, 1999, **60**, 2883.
20 J. L. Verble, T. J. Wietling and P. R. Reed, *Solid State Commun.*, 1972, **11**, 941.
21 L. Ma, J. Ye, W. Chen, J. Wang, R. Liu and J. Y. Lee, *ChemElectroChem*, 2015, **2**, 538.
22 T. Stephenson, Z. Li, B. Olsen and D. Mitlin, *Energy Environ. Sci.*, 2014, **7**, 209.

23 C. Zhu, X. Mu, P. A. van Aken, Y. Yu and J. Maier, *Angew. Chem.*, 2014, **53**, 2152.
24 W. F. Li, Y. M. Yang, G. Zhang and Y. W. Zhang, *Nano Lett.*, 2015, **15**, 1691.
25 K. Chang and W. Chen, *Chem. Commun.*, 2011, **47**, 4252.
26 K. Chang, W. Chen, L. Ma, H. Li, H. Li, F. Huang, Z. Xu, Q. Zhang and J.-Y. Lee, *J. Mater. Chem.*, 2011, **21**, 6251.
27 K. Chang and W. X. Chen, *ACS Nano*, 2011, **5**, 4720.
28 L. Fei, Y. Xu, X. Wu, G. Chen, Y. Li, B. Li, S. Deng, S. Smirnov, H. Fan and H. Luo, *Nanoscale*, 2014, **6**, 3664.
29 D. Xie, W. J. Tang, X. H. Xia, D. H. Wang, D. Zhou, F. Shi, X. L. Wang, C. D. Gu and J. P. Tu, *J. Power Sources*, 2015, **296**, 392.
30 K. S. Kumar, W. Li, M. Choi, S. M. Kim and J. Kim, *Chem. Eng. J.*, 2016, **285**, 517.
31 S. Hu, W. Chen, J. Zhou, F. Yin, E. Uchaker, Q. Zhang and G. Cao, *J. Mater. Chem. A*, 2014, **2**, 7862.
32 P. Sun, W. Zhang, X. Hu, L. Yuan and Y. Huang, *J. Mater. Chem. A*, 2014, **2**, 3498.
33 Z. Deng, Y. Hu, D. Ren, S. Lin, H. Jiang and C. Li, *Chem. Commun.*, 2015, **51**, 13838.
34 W. J. Zhu, H. Yang, W. K. Zhang, H. Huang, X. Y. Tao, Y. Xia, Y. P. Gan and X. Z. Guo, *RSC Adv.*, 2015, **5**, 74774.
35 H. Li, K. Yu, H. Fu, B. Guo, X. Lei and Z. Zhu, *J. Phys. Chem. C*, 2015, **119**, 7959.
36 W. J. Zhu, H. Yang and X. Z. Guo, *RSC Adv.*, 2016, **6**, 13505.
37 T. S. Sahu and S. Mitra, *Sci. Rep.*, 2015, **5**, 12571.
38 Z. Wang, T. Chen, W. X. Chen and J. Y. Lee, *J. Mater. Chem. A*, 2013, **1**, 2202.
39 A. Muller, S. Sarkar and M. Dartmann, *Angew. Chem.*, 1978, **90**, 535.
40 W. L. Lindsay and W. A. Norvell, *Soil Sci. Soc. Am. J.*, 1978, **42**, 421.